Front. Phys., 2012, 7(6): 721–727
DOI 10.1007/s11467-012-0254-z

RESEARCH ARTICLE

Temperature and electron density of soil plasma generated by LA-FPDPS

Xia-Fen Li[1], **Wei-Dong Zhou**[1,†], **Zhi-Feng Cui**[2]

[1] *The Institute of Information Optics, Zhejiang Normal University, Jinhua 321004, China*
[2] *Department of Physics, Anhui Normal University, Wuhu 241000, China*
E-mail: [†] *wdzhou@zjnu.cn*
Received March 15 2012; accepted May 17, 2012

Electron temperature and electron number density are important parameters in the characterization of plasma. In this paper the electron temperature and electron number density of soil plasma generated by laser ablation combined with nanosecond discharge spark at different discharge voltages have been studied. Saha–Boltzmann plot and Stark broadening are used to determine the temperature and electron number density. It is proved that local thermal equilibrium is fulfilled in the nanosecond spark enhanced plasma. The enhanced optical emission, signal to noise ratio and the stability in term of the relative standard deviation of signal intensity at different spark voltages were investigated in detail. A relative stable discharge process was observed with use of a 10 kV discharge voltage under the carried experimental configuration.

Keywords laser ablation fast pulse discharge plasma spectroscopy (LA-FPDPS), local thermodynamic equilibrium (LTE), electron temperature, electron number density, discharge voltage

PACS numbers 52.50.Jm, 52.80.Yr, 82.80.Dx

1 Introduction

Laser-induced breakdown spectroscopy (LIBS) technique is a fast developing analytical technique, which has acquired great interest in recent years and is becoming a well known real time analytical tool for rapid quantitative analysis of almost any type of material (solids, gases and liquids) [1–5]. In LIBS technique, the intensities of spectral lines are used to determine the concentrations of elements in an analyte. As the intensities of spectral line and continuum emission of the laser induced plasmas depends on the laser material interaction process and the physical characters of plasma, to investigate the characteristic physical parameters and understand the dynamics of plasma plume in order to achieve improvements in the applications of LIBS is therefore essential. The plasma temperature and the electron density are the two main parameters for plasma characterization. Based on the measured plasma temperature and electron number density, the calibration-free laser-induced breakdown spectroscopy was developed by Ciucci *et al.* [6], which in principle does not need a calibration curve for the elemental analysis, and has thus avoided the time consuming calibration experiments by using lots of standard samples and the matrix effect. Plasma temperature and electron density has also been used as a criterion for normalizing the spectral line intensities and improving measurement accuracy and repeatability (precision) in LIBS analysis, which was due to the fluctuations of experimental parameters and matrix effects [7].

The determination of plasma characters is an important task in the plasma characterization research. The principles for characterization of laser induced plasma by optical emission spectroscopy had been described in a review article by Adrain and Watson [8]. The laser plasma characterization and analytical applications, including the principles of laser plasma spectroscopy used for characterization and spectrochemical analysis had also been described in a book edited by Radziemski and Cremers [9]. Basically, the electron temperature of plasma can be determined from the emission spectrum of the plume [10] by using the Boltzmann and Saha equilibrium equations if local thermodynamic equilibrium is satisfied. In general, the temperature can simply be obtained by the two emission lines which have enough energy difference on their upper energy levels by using Boltzmann plot [11, 12]. The second way to determine the temperature is using Saha–Boltzmann plot, which is related to a bunch of emission lines of the neutral atom and the ion of a specific

element. The advantage of the Saha–Boltzmann plot as compared to the Boltzmann plot is that the lines between the neutral and ion has a wider range of the upper level energies, which will improve the accuracy of the measured temperature value. The electron number density plays an outstanding role in the study of the degree of thermodynamic equilibrium of the laser plasma. Its value makes it possible to establish how far the plasma is from the local thermodynamic equilibrium (LTE) conditions [13, 14], a critical pre-assumption for LIBS quantitative analysis. One of the most powerful spectroscopic techniques to determine the electron density with reasonable accuracy is by the measurements of the Stark broadening line profile of an isolated atom or singly charged ion [15, 16].

To date, LIBS has been widely applied for analytical purpose in many fields. With the intention to improve the performance of the LIBS technique, some combination methods of laser ablation with the secondary excitation source have been investigated in order to enhance the optical emission of laser plasma and to improve the signal-to-noise (S/N) ratio [17–27]. The combination of secondary excitation source with laser ablation can improve the homogeneity of plasma and increase the plasma lifetime and amount or lifetime of the luminous species, and generally will get a more stable signal and higher signal to noise ratio (SNR) compared with single pulse LIBS. The secondary excitation sources include another sequential laser pulses [17–19], electric spark discharges [20–24], radiofrequency [25, 26], and microwave radiation [27], etc.

Recently, a nanosecond discharge enhanced laser plasma source is developed [28, 29]. Preliminary experimental results indicate that the combination technique of laser ablation with a nanosecond discharge will greatly enhance the optical emission intensity of laser plasma of soil. Impressively, although a much lower discharge voltage (8 kV) is used in the nanosecond spark, the peak intensities obtained from the trace element lines of soil plasma emission were greatly enhanced when compared with the microsecond spark which uses a 11 kV discharge voltage. This character, a lower discharge voltage but a higher signal intensity, is very useful in practical application. In addition, the better precision in terms of relative standard deviations (RSD) and signal to noise ratios (S/N) were improved as well. The great advantage of using the nanosecond discharge circuit to increase the optical emission intensity and S/N ratio from laser ablated plasma is demonstrated. Similar to that of double pulse LIBS technique, it is likely that this technique will gain a practical application in the analysis that needs great sensitivity.

The plasma temperature and the electron density are the two most significant parameters of fundamental importance for the characterization of spectrochemical plasma sources. In addition, the electron number density makes it possible to establish how far the plasma is from the local thermodynamic equilibrium (LTE) conditions. Therefore, similar to that in LIBS technique, the investigation of the temperature and electron number density of discharge plasma is extremely necessary. In this article, the variation of the electron temperature and electron number density of plasma generated by laser ablation fast pulse discharge plasma spectroscopy (LA-FPDPS) technique using different nanosecond discharge voltage is investigated. In addition, the character of the signal enhancements has also been studied.

2 Method for temperature and electron density measurement

2.1 The Boltzmann plot

In an LTE approximation, the optically thin emission line integral intensity corresponding to the transition between two levels E_k and E_i of an atomic species is

$$I_\lambda^{ki} = N_s A_{ki} \frac{g_k \mathrm{e}^{-E_k/(k_\mathrm{B}T)}}{U_s(T)} \tag{1}$$

where λ is the wavelength of the transition; N_s is the total number density (cm^{-3}) of the species in the plasma; A_{ki} is the transition probability for the given line; g_k is the k level degeneracy [30].

In actual measurements, the efficiency of the collecting system affects as a scale factor the measured intensity of the line. So, the measured integral intensity is

$$I_\lambda^{ki} = F C_s A_{ki} \frac{g_k \mathrm{e}^{-E_k/(k_\mathrm{B}T)}}{U_s(T)} \tag{2}$$

where C_s represents the concentration of the emitting atomic species, and F is the experimental parameter which takes into account the plasma density, volume of plasma, the integration time as well as the optical efficiency of the collection system.

$U_s(T)$ is the partition function for the emitting species at the plasma temperature T:

$$U_s(T) = \sum_i g_k \mathrm{e}^{-E_k/(k_\mathrm{B}T)} \tag{3}$$

A_{ki}, E_k, and g_k can be retrieved from the National Institute for Standards and Technology (NIST) Database for Atomic Spectroscopy.

By taking the logarithm of both sides of Eq. (2), we obtain

$$\ln \frac{\overline{I_\lambda^{ki}}}{g_k A_{ki}} = \frac{-E_k}{k_\mathrm{B}T} + \ln \frac{F C_s}{U_s(T)} \tag{4}$$

We can define

$$y_i = \ln \frac{\overline{I_\lambda^{ki}}}{g_k A_{ki}}, \quad x_i = E_k, \quad m = -\frac{1}{k_\mathrm{B}T}$$

$$q_s = \ln \frac{C_s F}{U_s(T)} \tag{5}$$

From substituting the above definitions, we can obtain the following Boltzmann plot equation:

$$y_i = mx_i + q_s \tag{6}$$

The plasma temperature can be determined from the slope m of the Boltzmann plot.

The accuracy of the temperature measurement based on this method depends on the availability of spectral lines with large difference in the excitation energies of upper level. To receive a more accurate temperature one can use Saha–Boltzmann plot.

2.2 The Saha–Boltzmann plot

In the LTE assumption, the Saha–Boltzmann plot method can provide a reasonable estimation in cases of plasmas in LIBS [30–32] and in spark discharge [33]. The ratio between the singly ionized and neutral species of the same element can be calculated by

$$n_e \frac{n^{\mathrm{II}}}{n^{\mathrm{I}}} = \frac{(2\pi m_e k_{\mathrm{B}} T)^{3/2}}{h^3} \frac{2U^{\mathrm{II}}(T)}{U^{\mathrm{I}}(T)} \mathrm{e}^{-E_{\mathrm{ion}}/(k_{\mathrm{B}}T)} \tag{7}$$

where N_e is the electron density (cm^{-3}), E_{ion}(eV) is the ionization energy, m_e is the mass of the electron (g), h is the Planck constant (eV· s). Then according to the Eq. (7) the intensity of an ionic line I can be described as

$$I_\lambda^{\mathrm{II}} = n^{\mathrm{II}} A_{ki}^{\mathrm{II}} g_k^{\mathrm{II}} \frac{\mathrm{e}^{-E_k^{\mathrm{II}}/(k_{\mathrm{B}}T)}}{U_s^{\mathrm{II}}(T)} = A_{ki}^{\mathrm{II}} g_k^{\mathrm{II}} \frac{\mathrm{e}^{-E_k^{\mathrm{II}}/(k_{\mathrm{B}}T)}}{U^{\mathrm{I}}(T)} \cdot \frac{n^I}{n_e} \frac{2(2\pi m_e)^{3/2}}{h^3} (k_{\mathrm{B}}T)^{3/2} \mathrm{e}^{-E_{\mathrm{ion}}/(k_{\mathrm{B}}T)} \tag{8}$$

Then, taking the logarithm of the intensity of an ionic line, we obtain

$$\ln \frac{I_\lambda^{\mathrm{II}}}{A_{ki}^{\mathrm{II}} g_k^{\mathrm{II}}} = \ln \frac{FC^{\mathrm{I}}}{U^{\mathrm{I}}} + \ln \frac{2(2\pi m_e)^{3/2}(k_{\mathrm{B}}T)^{3/2}}{n_e h^3} - \frac{E_{\mathrm{ion}} + E_k^{\mathrm{II}}}{k_{\mathrm{B}}T} \tag{9}$$

On the basis of the Boltzmann method, we can obtain

$$x^* = \begin{cases} E_k & \text{for neutral lines} \\ E_j + E_{\mathrm{ion}} & \text{for ionic lines} \end{cases}$$

$$y^* = \begin{cases} \ln \dfrac{I_{ki}}{A_{ki} g_k} & \text{for neutral lines} \\ \ln \dfrac{I_{jh}}{A_{jh} g_i} - \ln \dfrac{2(2\pi m_e)^{3/2}(k_{\mathrm{B}}T)^{3/2}}{n_e h^3} & \text{for ionic lines} \end{cases} \tag{10}$$

So Eq. (9) can be described as follows:

$$y^* = mx^* + q_s \tag{11}$$

Similar to that of Boltzmann plot, a straight line is then achieved and is called Saha–Boltzmann plot. And the slope m of the plot is related to the electron temperature as well.

2.3 Electron density

One of the most powerful spectroscopic techniques to determine the electron number density with reasonable accuracy is by the measurements of the Stark broadened line profile of an isolated atom or singly charged ion. The Stark broadening, Doppler broadening, and pressure broadening will affect the observed line widths. And the Stark broadening is the primary mechanism influencing the plasma emission spectra [34].

The electron number density N_e in cm^{-3} related to Stark broadening lines is given by [35]

$$\Delta\lambda_{1/2} = 2\omega \cdot \frac{N_e}{10^{16}} + 3.5A \left(\frac{N_e}{10^{16}}\right)^{1/4} \cdot (1 - 1.2N_{\mathrm{D}}^{-1/3})\omega \cdot \frac{N_e}{10^{16}} \cdot A \tag{12}$$

where ω is the electron impact parameter (nm), A is the ion broadening parameter (nm) and N_{D} is the number of particles in the Debye sphere, $\Delta\lambda_{1/2}$ is the FWHM of Stark broadening lines. The second term of the ionic broadening is so small that can be neglected from Eq. (12) and the electron density N_e can be given by the formula:

$$\Delta\lambda_{1/2} = 2\omega \cdot \frac{N_e}{10^{16}} \tag{13}$$

In the LIBS analysis the line shapes are often fitted with pure Lorentz distributions [36, 37] ($\Delta\lambda_{\mathrm{fit}}$). But when using the fitted line width to calculate the Stark broadening line width, one has to take care of the influence of the instrumental broadening.

And the actual calculation process of the Stark line width $\Delta\lambda_{1/2}$ for electron density calculations will be extracted by [38]

$$\Delta\lambda_s = \sqrt{\Delta\lambda_{\mathrm{fit}}^2 - \Delta\lambda_{\mathrm{ins}}^2} \tag{14}$$

where $\Delta\lambda_{\mathrm{fit}}$ is the Lorentz fit line width of the spectral line, $\Delta\lambda_{\mathrm{ins}}$ is the instrumental line width. The instrumental line width $\Delta\lambda_{\mathrm{ins}}$ of our Avantes Spectrometer system was found to be 0.1 nm with use of a low pressure mercury lamp in our experiment.

The McWhirter criterion provides the lower limit for the electron number density at which the plasma will be in LTE [39]

$$N_e \geqslant 1.6 \times 10^{12} T_e^{1/2} \Delta E^3$$

ΔE is the largest energy transition for which the condition holds and T_e is the excitation temperature.

3 Experimental

The experimental apparatus (Fig. 1) has been described in detail in references [20–22, 28]. Briefly, the LA-FPDPS system includes three major parts, a high voltage fast discharge circuit, a Q-switched pulse Nd:YAG laser and a spectroscopy detection system which is composed of a pulse generator and an Avaspec-2048 fiber optic Spectrometer. The pulse laser system and the spectroscopy detection system are similar with those used in a traditional single pulse LIBS system. The detector of the spectrometer was a CCD linear array having 2048 pixels, which can be externally triggered to start signal integration with an integrating time of 2 ms. The spectrometer was able to measure a wavelength range (196–500 nm) simultaneously with a spectral resolution of ∼0.1 nm.

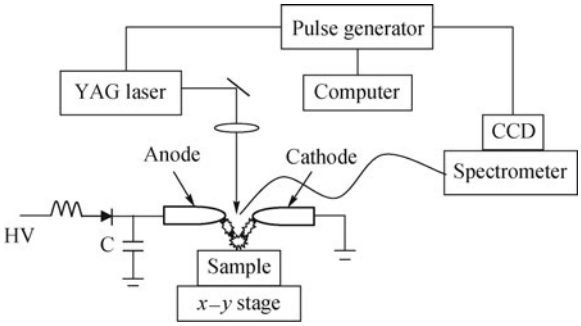

Fig. 1 Schematic diagram of LA-FPDPS system. HV – High voltage.

The high voltage and fast discharge circuit is composed of a high DC power supply coupled to a spark gap. The gap between the pair alloy electrodes is 5mm and has been set at a distance of 2 mm above the sample surface. The electrodes are cylindrical rods of 5 mm in diameter with a hemisphere shaped tip. A low inductive 6 nF capacitor is directly connected to the two electrodes. And the high voltage will add to the spark gap immediately when the capacitor was charged. The voltage used in the experiments is 8–11 kV. The circuit will give a rapid and time damped alternating electric discharge with a short oscillating period of ∼ 200 ns [28, 29]. Shortly after the sample was ablated by a focused Nd:YAG laser beam which comes typically 49 mJ per pulse at 1064 nm with a 10 ns pulse width, a discharge between electrodes was triggered automatically by the charged particles in the laser plasma. The expanding laser induced plume was then intercepted by the microsecond discharge spark. Then plasma emissions were collected and detected by an Avaspec-2048 fiber optic spectrometer.

All experiments were performed in the normal atmospheric condition. In the experiments, the sample is mounted on an x–y translation stage driven by two stepmotors so that the sample is moved during the data acquisition to ensure a fresh spot for each laser shot and discharge. The laser energy used in the experiments was 49 mJ per pulse.

4 Results and discussion

4.1 Optimization of discharge voltage

In the present work, the standard powder sample (GBW07419) from The National Institute of Metrology of China was used. In the measurements, the laser energy was ∼ 49 mJ. Figure 2 is the typical LA-FPDPS spectra obtained from soil sample at different discharge voltages from 8 kV to 11 kV and the traditional LIBS spectra, i.e., $V = 0$. Apparently, the LA-FPDPS spectral line intensity is greater than the simple LIBS spectra and it increases as the voltage rises. The RSD and the SNR of the line intensities of the averaged spectrum at different discharge voltages are shown in Table 1 and Table 2. As we found out, the stability of the spectra increases with the rise of the voltage, then decrease when the voltage gets greater than 10 kV. For the SNR of the spectra, it is smaller at 10 kV but close to that at 9 kV, indicating that a relatively stable discharge and spectral line intensity were obtained at a discharge voltage about 10 kV.

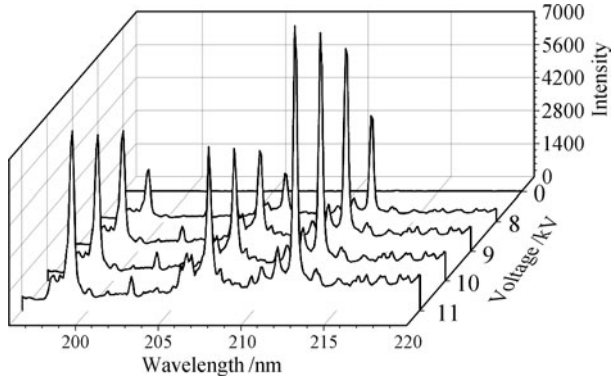

Fig. 2 Spectrum of soil sample obtained by LA-FPDPS at 8–11 kV discharge voltages.

Table 1 The RSD of a certain spectral lines with different discharge voltages.

	212.47	220.86	221.23	221.78	243.61	298.94	386.36	462.17	504.52
0 kV	0.0718	0.0988	0.0730	0.0592	0.0273	0.0456	0.0847	0.3050	0.1907
8 kV	0.0689	0.0654	0.0659	0.0659	0.0674	0.0624	0.0572	0.0521	0.0525
9 kV	0.0136	0.0143	0.0145	0.0148	0.0126	0.0156	0.0100	0.0101	0.0061
10 kV	0.0111	0.0080	0.0091	0.0089	0.0104	0.0067	0.0084	0.0015	0.0026
11 kV	0.0214	0.0177	0.0186	0.0206	0.0069	0.0150	0.0103	0.0094	0.0085

Table 2 The SNR of a certain spectral lines with different discharge voltages.

	212.47/nm	221.78/nm	250.8/nm	385.7/nm	462.17/nm
8kV	29.11	59.05	76.59	35.75	108.1
9kV	56.07	136.2	99.37	18.81	98.05
10kV	61.55	115.9	97.62	15.73	82.36
11kV	50.67	110.3	95.57	12.36	79.52

4.2 Electron temperature and electron number density

From the atomic and ionic Si line intensities of the measured spectra, after the correction of the measured line intensities for the spectral response of the optical system, a Saha–Boltzmann plot may be constructed. Table 3 shows the spectral parameters which are used in the temperature calculation. Figures 3(a)–7(a) are the Saha–Boltzmann plots and the deduced temperatures at different discharge voltages. The measured temperatures at different discharge voltages are listed in Table 4. Obviously, the electron temperature of the LA-FPDPS plasma is larger than the simple LIBS laser plasma in agreement with the enhanced optical emission in the LA-FPDPS technique. But the temperature has merely a slight variation with the increment of discharge voltage. The stark broadening of Si I 212.47 nm was used to calculate electron number density in the study. Figures 3(b)–7(b) shows the fitting of spectral profile of Si I 212.47 nm line in different discharge voltages. According to Eq. (14), the stark width can be derived, and the electron density can then be deduced from Eq. (13). In the stark line width measurements, the instrumental line width was measured by using low-pressure mercury lamp, and the value is about 0.1 nm. The measured electron number density at different discharge voltages are

Table 3 Parameters of Si emission lines for electron temperature calculations. (I, Neutral; II, Singly ionized)

	λ_{ki}/nm	E_k/eV	g_k	$A_{ki}/(10^8\mathrm{s})$
Si I	212.41	53362.24	7	2.97
	220.80	45276.19	3	0.26
	221.17	45276.19	3	0.18
	221.67	45321.845	7	0.45
	243.50	47351.55	5	0.44
	250.69	39955.05	5	0.55
	251.61	39955.05	5	1.68
	251.92	39760.29	3	0.55
	252.41	39683.16	1	2.22
	252.85	39760.29	3	0.90
	263.13	53387.33	3	1.06
	288.16	40991.88	3	2.17
	298.76	39760.28	3	0.01
Si II	207.20	103556.16	6	0.96
	385.60	81251.32	4	0.44
	386.26	81191.34	2	0.39
	413.09	103556.03	8	1.74
	504.10	101023.05	4	0.70

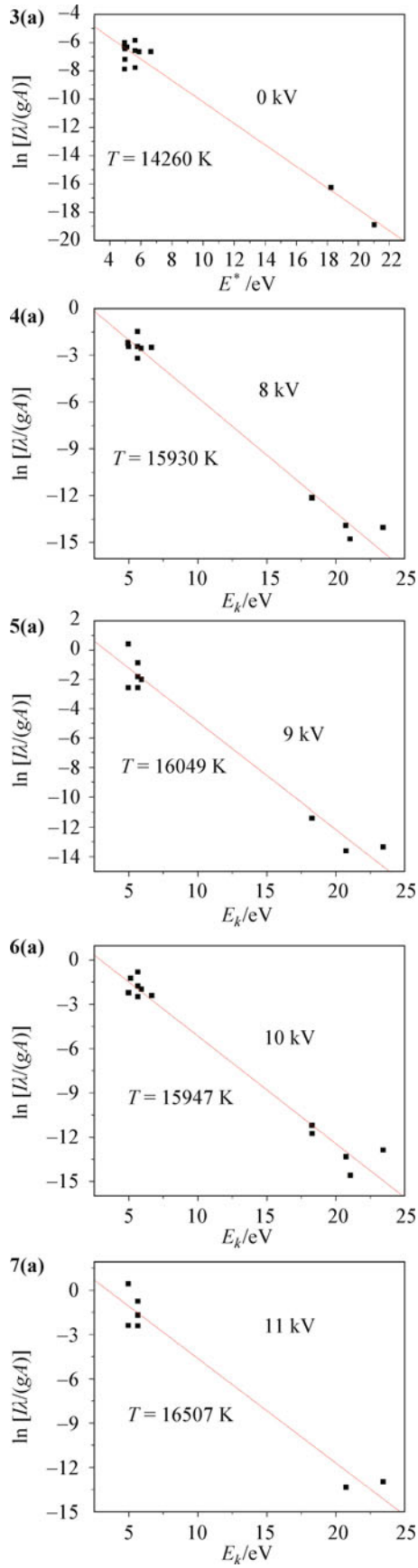

Figs. 3(a)–7(a) Saha–Boltzmann plot calculated from Si lines of soil plasma generated by LA-FPDPS.

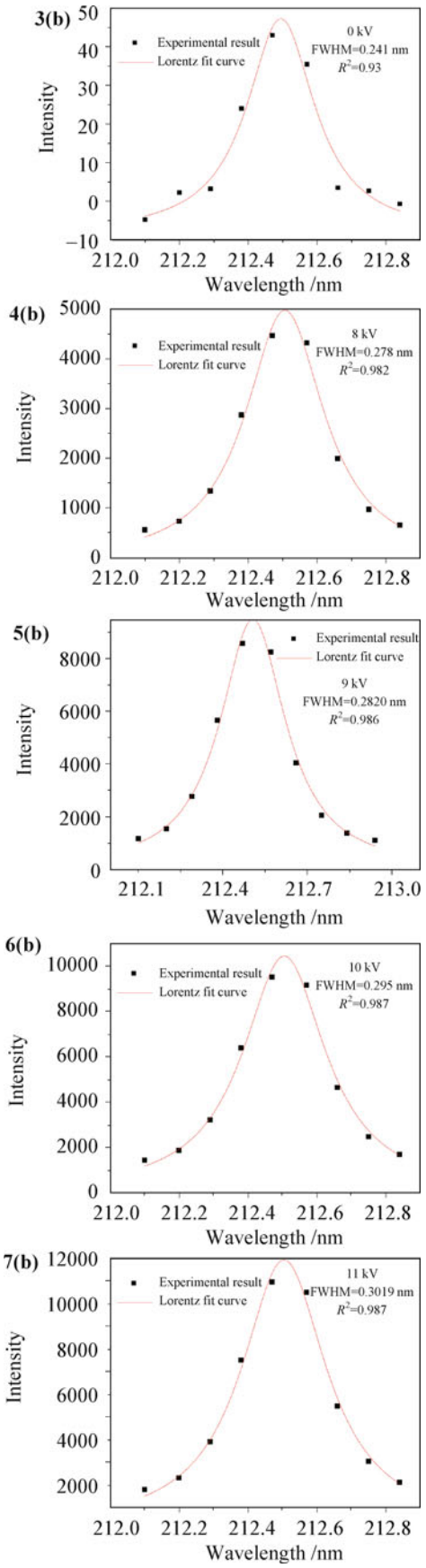

Figs. 3(b)–7(b) The fitting of spectral line profile of Si (I) transition at 212.47 nm.

listed in Table 4 as well. Similar to that of temperature, the electron number densities are higher in the LA-FPDPS plasma than that in the laser induced plasma. In addition, the electron number density monotonically increases with an increase of discharge voltage.

Table 4 The measured electron temperature (T) and electron number density (N_e) at different discharge voltages.

Discharge voltage/kV	T/K	$\omega/(10^{-3}\text{nm})$	$\Delta\lambda$/nm	$N_e/(10^{18}\text{cm}^{-3})$
0	14260	1.38	0.241	0.79
8	15930	1.25	0.278	1.04
9	16049	1.24	0.282	1.06
10	15947	1.24	0.295	1.12
11	16507	1.23	0.302	1.16

Note: ω is the electron impact parameter; $\Delta\lambda$ is the measured line width.

5 Conclusions

In summary, LTE condition is fulfilled in the soil spark plasma generated by LA-FPDPS, and the electron temperature and the electron number density in different discharge voltages have been measured. By comparing the enhancement of emission, the RSD, and the SNR of spectral line intensity, a relatively stable optical emission spectrum is found at a discharge voltage of 10 kV. The electron temperature and the electron number density of the spark plasma are larger than the simple LIBS laser plasma, in consistency with the finding that the intensity of spark spectral lines is greater than the LIBS lines. In addition, the electron temperature and the electron number density have been slightly incremented with the rise of discharge voltage as well.

Acknowledgements This work was supported by the National Natural Science Foundation of China (Grant No. 61178034), Zhejiang Provincial Natural Science Foundation of China (Grant No. Y1100268), and partially supported by Key Research Project of University of Zhejiang Province, China (Grant No. ZD2009006), and the Program for Innovative Research Team, Zhejiang Normal University, Jinhua, Zhejiang Province, China.

References

1. J. P. Singh and S. N. Thakur, Laser Induced Breakdown Spectroscopy, Elsevier, 2007
2. J. P. Singh, F. Y. Yueh, H. Zhang, and K. P. Karney, Recent Res. Dev. Appl. Spectrosc., 1999, 2: 59
3. V. N. Rai, A. K. Rai, F. Y. Yueh, and J. P. Singh, Appl. Opt., 2003, 42(12): 2085
4. H. Huang, Q. Chen, and W. Zhou, Spectrosc. Spectral Anal., 2009, 29: 3126
5. Z. Wang, J. Feng, L. Z. Li, W. Ni, and Z. Li, J. Anal. At. Spectrom., 2011, 26(11): 2175
6. A. Ciucci, M. Corsi, V. Palleschi, S. Rastelli, A. Salvetti, and E. Tognoni, Appl. Spectrosc., 1999, 53(8): 960
7. J. Feng, Z. Wang, Z. Li, and W. D. Ni, Spectrochim. Acta.

B, 2010, 65: 549

8. R. S. Adrain and J. Watson, J. Phys. D, 1984, 17(10): 1915
9. L. J. Radziemski and D. A. Cremers, Laser-Induced Plasmas and Applications, Marcel Dekker, 1989
10. E. tognoni, G. Cristoforetti, S. Legnaioli, V. Palleschi, and A. Salvetti, Spectrochim. Acta. B, 2007, 62: 1287
11. M. Essien, L. J. Radziemsky, and J. Sneddon, J. Anal. At. Spectrom., 1988, 3(7): 985
12. M. R. Joseph, N. Xu, and V. Majidi, Spectrochim. Acta. B, 1994, 49: 89
13. J. A. M. van der Mullen, Phys. Rep., 1990, 191(2–3): 109
14. M. D. Calzada, M. Moisan, A. Gamero, and A. Sola, J. Appl. Phys., 1996, 80(1): 46
15. J. A. Aguilera and C. Aragon, Specrochim. Acta. B, 2009, 64: 685
16. J. A. Aguilera and C. Aragon, Appl. Surf. Sci., 2002, 197–198: 273
17. L. St-Onge, M. Sabsabi, and P. Cielo, Spectrochim. Acta. B, 1998, 53: 407
18. T. Ctvrtníkova, L. M. Cabalín, J. Laserna, and V. Kanický, Spectrochim. Acta. B, 2008, 63: 42
19. V. I. Babushok, F. C. Jr DeLucia, J. L. Gottfried, C. A. Munson, and A. W. Miziolek, Spectrochim. Acta. B, 2006, 61: 999
20. K. X. Li, W. D. Zhou, Q. M. Shen, J. Shao, and H. G. Qian, Spectrochim. Acta. B, 2010, 65: 420
21. K. X. Li, W. D. Zhou, and Q. M. Shen, J. Anal. At. Spectrom., 2010, 25: 1475
22. W. D. Zhou, K. X. Li, Q. M. Shen, Q. L. Chen, and J. M. Long, Opt. Express, 2010, 18(3): 2573
23. Y. Chen, Q. Zhang, G. Li, R. Li, and J. Zhou, J. Anal. At. Spectrom., 2010, 25(12): 1969
24. O. A. Nassef and H. E. Elsayed-Ali, Spectrochim. Acta. B, 2005, 60: 1564
25. W. Deng, Y. Liu, G. Wei, X. Li, X. Tu, L. Xie, H. Zhang, and W. Sun, J. Anal. At. Spectrom., 2010, 25(1): 84
26. Q. Z. Bian, J. Koch, H. Lindner, H. Berndt, R. Hergenröder, and K. Niemax, J. Anal. At. Spectrom., 2005, 20(8): 736
27. Y. Ikeda, A. Moon, and M. Kaneko, Appl. Opt., 2010, 49(13): C95
28. W. D. Zhou, K. X. Li, X. F. Li, H. G. Qian, J. Shao, X. D. Fang, P. H. Xie, and W. Q. Liu, Opt. Lett., 2011, 36(15): 2961
29. W. D. Zhou, K. X. Li, H. G. Qian, Z. J. Ren, and Y. Yu, Appl. Opt., 2012, 51(7): B42
30. J. A. Aguilera and C. Aragon, Spectrochim. Acta. B, 2004, 59(12): 1861
31. L. J. Radziemski, T. R. Loree, D. A. Cremers, and N. M. Hoffman, Anal. Chem., 1983, 55(8): 1246
32. M. Milan and J. J. Laserna, Spectrochim. Acta. B, 2001, 56: 275
33. C. A. Bye and A. Schheeline, Appl. Spectrosc., 1993, 47(12): 2022
34. X. Z. Zeng, S. S. Mao, C. Y. Liu, X. L. Mao, R. Greif, and R. E. Russo, Spectrochim. Acta. B, 2003, 58: 867
35. H. R. Griem, Plasma Spectroscopy, New York: McGraw-Hill, 1964: 483
36. C. A. Bye and A. Scheeline, J. Quant. Spectrosc. Radiat. Trans., 1995, 53(1): 75
37. J. Hermann, C. Boulmer-Leborgne, and D. Hong, J. Appl. Phys., 1998, 83(2): 691
38. F. Colao, R. Fantoni, V. Lazic, and A. Paolini, Appl. Phys. A, 2004, 79(1): 143
39. R. W. P. McWhirter, Plasma Diagnostic Techniques, New York: Academic Press, 1965, Chap. 5: 206